

Out-of-Distribution Semantic Occupancy Prediction

Yuheng Zhang^{1,*} Mengfei Duan^{1,*} Kunyu Peng^{2,†} Yuhang Wang¹ Ruiping Liu²
 Fei Teng¹ Kai Luo¹ Zhiyong Li¹ Kailun Yang^{1,†}
¹Hunan University ²Karlsruhe Institute of Technology

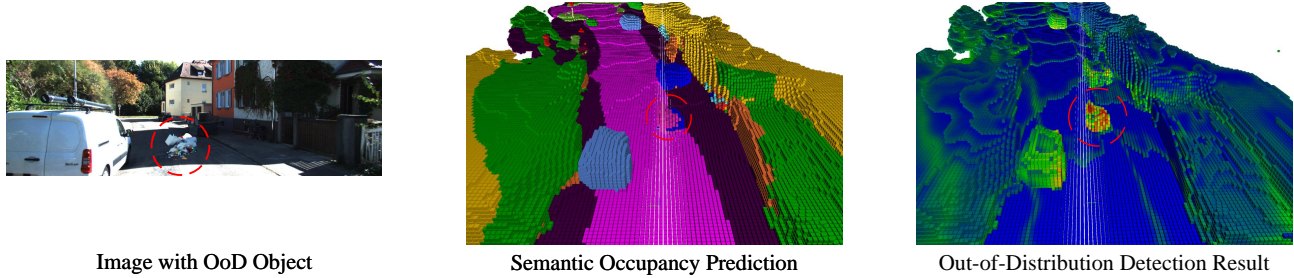


Figure 1. Visualization of the established task of **Out-of-Distribution Semantic Occupancy Prediction**. The mainstream semantic occupancy prediction method tends to misclassify Out-of-Distribution (OoD) objects as inliers, thus endangering the safety of autonomous driving. Our proposed OccOoD solution accurately identifies OoD objects, with anomaly scores visualized from low (blue) to high (red).

Abstract

3D Semantic Occupancy Prediction is crucial for autonomous driving, providing a dense, semantically rich environmental representation. However, existing methods focus on in-distribution scenes, making them susceptible to Out-of-Distribution (OoD) objects and long-tail distributions, which increases the risk of undetected anomalies and misinterpretations, posing safety hazards. To address these challenges, we introduce Out-of-Distribution Semantic Occupancy Prediction, targeting OoD detection in 3D voxel space. To fill the gaps in the dataset, we propose a Synthetic Anomaly Integration Pipeline that injects synthetic anomalies while preserving realistic spatial and occlusion patterns, enabling the creation of two datasets: VAA-KITTI and VAA-KITTI-360. We introduce OccOoD, a novel framework integrating OoD detection into 3D semantic occupancy prediction, with Voxel-BEV Progressive Fusion (VBPF) leveraging an RWKV-based branch to enhance OoD detection via geometry-semantic fusion. Experimental results demonstrate that OccOoD achieves state-of-the-art OoD detection with an AuROC of 67.34% and an AuPRC_r of 29.21% within a 1.2m region, while maintaining competitive occupancy prediction performance. The established datasets and source code will be made publicly available at <https://github.com/7uHeng/OccOoD>.

1. Introduction

3D scene understanding is fundamental to autonomous driving, crucial for motion planning and obstacle avoidance [36]. The cost-effectiveness and ease of deployment of cameras have made vision-based 3D understanding methods a focal point of research [12, 37, 53, 62, 66, 82, 97, 114, 121]. Among these methods, 3D semantic occupancy prediction networks [41, 51, 66] are distinguished by their ability to accurately reconstruct geometry and semantic details. By producing detailed occupancy maps with rich semantic context, these networks improve environmental perception and decision-making, enhancing the safety and reliability of autonomous navigation.

However, current methods [41, 51, 85] primarily focus on in-distribution scenarios, where models are trained and evaluated on predefined object categories and environments. While effective in controlled settings, this approach [12, 53] exposes systems to vulnerabilities from OoD objects and anomalies commonly encountered in real-world scenarios [8, 17, 33, 55], as seen in Fig. 1 where the standard semantic occupancy prediction method [66] produces misclassifications. OoD detection—the capability to identify entities that substantially deviate from the training data distribution—remains a critical yet underexplored challenge. Such anomalies include unexpected obstacles (e.g., discarded furniture, stray wildlife, construction equipment), unusual road conditions (e.g., potholes, debris, or oil spills), and atypical weather phenomena (e.g., sudden fog, heavy rain, or snowdrifts). As existing systems may misinterpret or fail to detect these deviations, they pose significant safety

*Equal contribution

†Correspondence: kunyu.peng@kit.edu, kailun.yang@hnu.edu.cn

risks, potentially leading to failures and even catastrophic consequences in autonomous driving.

To bridge this critical gap, we introduce the task of Out-of-Distribution Semantic Occupancy Prediction. However, a key challenge in this domain is the scarcity of datasets annotated for both semantic occupancy and OoD anomalies, hindering robust model development. To address this, we propose a *Synthetic Anomaly Integration Pipeline* that injects diverse anomalies into existing datasets while preserving realistic spatial and occlusion patterns. This pipeline enables the creation of two novel datasets comprising 26 distinct categories of anomalies, where anomaly annotations encompass a diverse range of unforeseen hazards, facilitating comprehensive evaluation of OoD detection in 3D scene understanding. Building upon our newly proposed datasets for out-of-distribution detection in semantic occupancy prediction, we introduce OccOoD, the first unified framework that seamlessly integrates OoD detection into 3D semantic occupancy prediction.

OccOoD incorporates several key innovations to enhance anomaly detection in complex environments. First, existing methods [51, 66] rely on a single-voxel representation, which limits the effectiveness of OoD detection. To address this, we propose a Voxel-BEV Progressive Fusion strategy, which integrates voxel-based and Bird’s-Eye-View (BEV) representations. BEV enhances global scene understanding, enabling improved occupancy prediction and robust OoD detection. Second, we introduce a dedicated OoD detection mechanism leveraging entropy and cosine similarity, enabling effective identification of anomalies in dynamic and unstructured scenes. Finally, to ensure comprehensive evaluation, we conduct extensive OoD detection experiments on the newly proposed datasets and verify our occupancy prediction performance based on public benchmarks. The experimental results show that OccOoD achieves AuROC scores of 65.91% and 67.34% on the two proposed datasets, respectively, and attains mIoU scores of 15.85% and 18.37% on SemanticKITTI [3], and KITTI-360 [52], respectively. These results collectively establish OccOoD as a robust and scalable solution for addressing OoD challenges in 3D semantic occupancy prediction.

In a nutshell, our contributions are three-fold:

- We for the first time introduce out-of-distribution detection into the task of semantic occupancy prediction by delivering two new datasets VAA-KITTI and VAA-KITTI-360, specifically designed to evaluate out-of-distribution detection in the context of autonomous driving safety.
- We propose OccOoD, a multi-view fusion framework that integrates front-view and bird’s-eye-view representations, enabling a comprehensive spatial understanding of outliers and seamless integration of OoD detection into 3D semantic occupancy prediction. This framework robustly handles both known and unknown objects.

- Our proposed framework, OccOoD, achieves state-of-the-art OoD detection performance on the established datasets while maintaining competitive accuracy in 3D semantic occupancy prediction.

2. Related Work

Semantic Occupancy Prediction. 3D Semantic Occupancy Prediction aims to infer both the geometry and semantics of a scene by inferring the occupancy state of voxels [19, 73, 79, 100, 105]. To advance estimation quality and efficiency, efforts are made in 3D representation [23, 35, 39, 42, 44, 49, 56, 61, 62, 78, 82, 98, 117], context enhancement [46, 48, 86, 89, 96, 101, 124], modality fusion [14, 30, 64, 70, 75, 104, 113, 120], temporal association [11, 69, 91, 92, 108, 109], long-sequence and generative modeling [47, 54, 85, 90, 123], self-supervision [9, 10, 32, 38, 71], and offboard processing [40, 63, 77, 94, 118]. These efforts have collectively improved the quality and efficiency of semantic occupancy prediction. Recently, several works [41, 66, 110, 121] have introduced more fine-grained feature processing techniques. Meanwhile, uncertainty-aware methods [13, 80, 93] incorporate uncertainty quantification to enhance estimation reliability. However, these methods are limited to predefined categories, requiring retraining to generalize to novel object types and lacking flexibility. While open-vocabulary learning [9, 81, 87, 116, 119] addresses generalization to arbitrary categories, it remains constrained to In-Distribution (ID) scenarios and fails to handle OoD detection. In real-world applications, the categories of anomalous objects are unforeseeable, making such methods less reliable. In contrast, our proposed model extends semantic occupancy prediction by perceiving all OoD objects, enabling efficient and comprehensive OoD detection.

Out-of-Distribution Segmentation. Out-of-distribution segmentation identifies anomalies in specific scenes [8, 17, 22, 55] while maintaining in-distribution segmentation capabilities. Current research primarily focuses on anomaly detection in 2D images of road scenes, with the main methods including per-pixel architectures and mask-transformer-based approaches [1, 25, 29, 68, 74]. The per-pixel architecture methods include uncertainty-based [16, 21, 33, 43, 67], reconstruction-based [27, 31, 55, 88, 99], and outlier exposure [18, 20, 28, 58, 84] methods. Although these methods have advanced 2D anomaly detection, they are limited to narrow field-of-view pinhole cameras, hindering their application to complex 3D scenarios requiring high-precision spatial perception. Some studies extend anomaly detection to 3D space; however, these efforts primarily focus on industrial [5, 57] or indoor object defect detection [7, 50], where models fuse static point cloud data to optimize defect localization [4, 15, 34, 111, 122]. Due to reliance on geometric consistency assumption of static objects and lim-

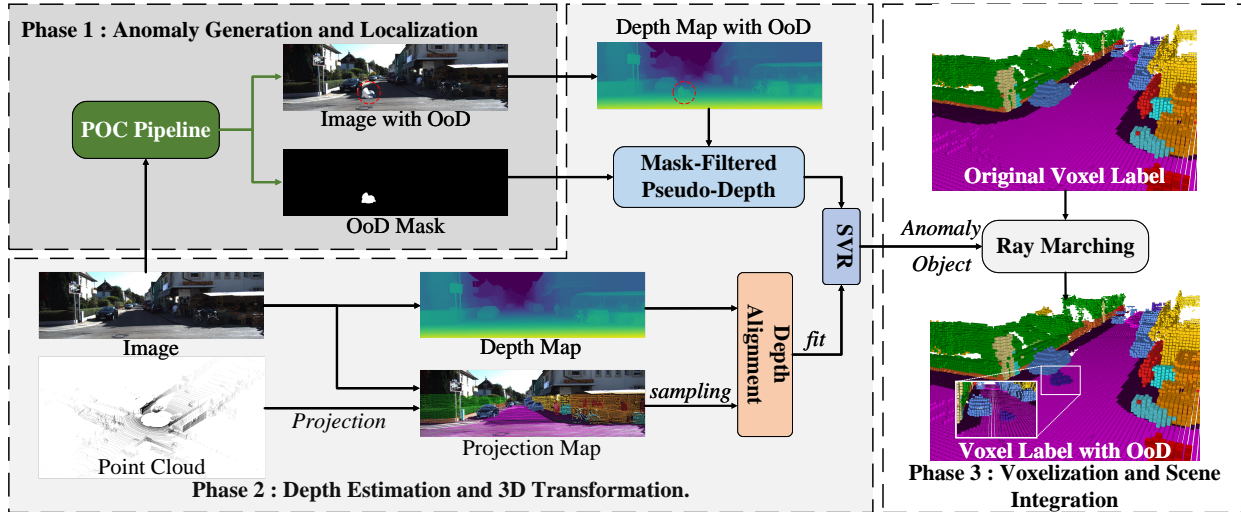


Figure 2. An illustration of the proposed Synthetic Anomaly Integration Pipeline. This pipeline is designed to address the challenges of collecting real-world OoD data by synthesizing anomalies that are both physically plausible and contextually realistic.

ited sensitivity to dynamic changes, these methods fail to meet the demands of more complex scenarios. In comparison, our work introduces OoD segmentation into vision-based 3D semantic occupancy prediction, overcoming the limitations of current methods in dynamic environments.

3. Out-of-Distribution Datasets

We introduce the task of Out-of-Distribution Semantic Occupancy Prediction. To address the lack of evaluation platforms, we propose a *Synthetic Anomaly Integration Pipeline* to generate abnormal objects in real road scene images, leading to the creation of two novel datasets: **VAA-KITTI** and **VAA-KITTI-360**.

3.1. Synthetic Anomaly Integration Pipeline

Collecting images and point cloud data of OoD objects is challenging due to their rarity in real-world scenes and the high cost of data collection and annotation. To address this, we propose a *Synthetic Anomaly Integration Pipeline* that generates synthetic anomalies under physical and environmental constraints, ensuring plausibility and challenge for robust OoD detection model evaluation. As illustrated in Fig. 2, our pipeline is structured into three key phases:

Phase 1: Anomaly Generation and Localization. In 2D anomaly detection, studies have demonstrated that synthetic anomaly data is highly effective for model training and evaluation [24, 59]. We employ POC [24], a state-of-the-art image generation technique, to synthesize anomaly images and their corresponding mask maps, enabling precise localization of anomalous objects. To better align with real-world application scenarios, we introduce multi-category anomalies into the images, as shown in Fig. 3.

Phase 2: Depth Estimation and 3D Transformation.

This phase focuses on integrating image data with accurate depth information, facilitating the transformation of 2D anomaly detection results into precise 3D spatial localization. To address the challenge of limited metric depth estimation accuracy, we propose a method to project synthesized anomalies into the 3D point cloud.

We first utilize the large version of Depth Anything V2 [103], a state-of-the-art depth estimation model, to compute pseudo-depth for both original and synthesized images. Subsequently, we randomly sample a predefined number of points, from the point cloud and project them onto the image plane to obtain pixel coordinates \mathbf{u}_i and Euclidean distances d_i as:

$$\mathbf{u}_i = \frac{\mathbf{K} \cdot (\mathbf{R}\mathbf{p}_i + \mathbf{t})}{[\mathbf{R}\mathbf{p}_i + \mathbf{t}]_z}, \quad (1)$$

$$d_i = \|\mathbf{R}\mathbf{p}_i + \mathbf{t}\|_2,$$

where \mathbf{p}_i is a 3D point, \mathbf{K} is the camera intrinsic matrix, \mathbf{R} and \mathbf{t} are the rotation and translation of the camera, \mathbf{u}_i is the projected 2D point, and d_i is the Euclidean distance.

By utilizing \mathbf{u}_i and the previously obtained depth map, we align the pseudo-depth with the real depth and apply Support Vector Regression (SVR) [2] for nonlinear regression, mapping the pseudo-depth to real-world depth. Finally, the aligned depth map and mask map from Phase 1 are used to derive 3D anomaly coordinates (u, v, d) , which are then transformed into the 3D voxel space.

Phase 3: Voxelization and Scene Integration. The pseudo-point clouds of anomalies are voxelized and integrated into the 3D voxel space of the original point cloud. Leveraging camera poses, we project each anomaly point $\mathbf{A}_i^v = (x_i^v, y_i^v, z_i^v)$ (representing the discrete voxel coordinates of the i -th anomaly) back into the scene to determine

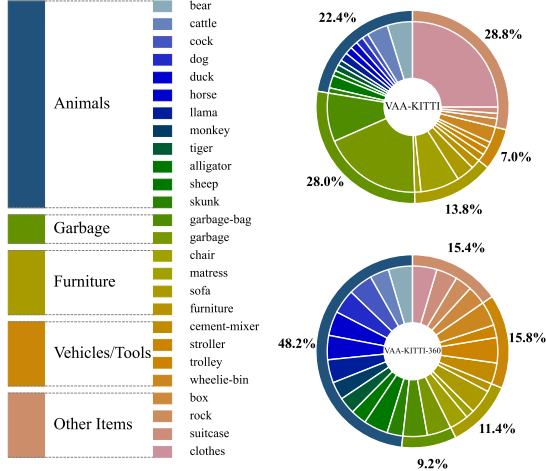


Figure 3. Distribution map of VAA-KITTI and VAA-KITTI-360 datasets. The datasets contain 26 distinct OoD categories, which can be divided into five main categories as shown in the figure.

occlusion relationships via ray marching. The ray position of the ray at step k is computed as:

$$\mathbf{c}_k = \mathbf{C}^v + k \cdot \frac{\mathbf{A}_i^v - \mathbf{C}^v}{\|\mathbf{A}_i^v - \mathbf{C}^v\|_2}, \quad (2)$$

where k is the step index, \mathbf{c}_k is the ray position at k , \mathbf{C}^v is the camera position and $\mathbf{v}_k = \text{round}(\mathbf{c}_k)$ is the corresponding voxel center. The step size is controlled by a scaling factor $s > 0$, with $\Delta = \frac{1}{s}$ defining the resolution.

The occlusion process is formalized as:

$$\mathbf{V}[\mathbf{v}_k] = \begin{cases} 1, & \text{if } \|\mathbf{c}_k - \mathbf{A}_i^v\|_2 \leq \Delta, \\ 0, & \text{otherwise.} \end{cases} \quad (3)$$

where 0 and 1 represent the occupancy status of the voxel.

3.2. VAA-KITTI and VAA-KITTI-360

We applied the aforementioned synthesis pipeline to the SemanticKITTI [3] and SSCBench-KITTI-360 [52] datasets, resulting in the creation of two new synthetic datasets: VAA-KITTI and VAA-KITTI-360. These synthesized datasets extend the original label sets by introducing anomaly labels, encompassing 26 distinct categories of anomalies such as *animals*, *furniture*, and *garbage bags*.

To ensure the plausibility and naturalness of the generated images, over 30,000 images produced using the POC algorithm were carefully reviewed by three independent annotators. After multiple rounds of cross-validation, images with poor generation quality, implausible object placements, or non-anomalous scenarios (e.g., birds flying in an urban sky or trash, trash bags, and wheeled bins placed alongside sidewalks) are excluded, resulting in a final selection of 500 images for both the VAA-KITTI and VAA-KITTI-360 datasets to form the test set for the Out-of-Distribution Semantic Occupancy Prediction task.

Regional-Level Metrics Design: Referring to the field of 2D image anomaly detection, we adopt Area under the Receiver Operating Characteristic Curve (AuROC) as one of the evaluation metrics for model performance. Furthermore, to mitigate the evaluation impact caused by the inaccuracy of existing methods in predicting the absolute positions of instances, and bridge the gap between localization demands and anomaly-awareness goals, we propose a regional-level evaluation metric: Regional Area under the Precision-Recall Curve (AuPRC_r). The AuPRC_r incorporates tolerance for minor localization inaccuracies while maintaining sensitivity to anomaly detection.

AuPRC_r: The Precision-Recall (PR) curve evaluates the balance between precision and recall at varying thresholds:

$$\text{Precision}_r = \frac{\text{TP}_r}{\text{TP}_r + \text{FP}_r}, \quad \text{Recall}_r = \frac{\text{TP}_r}{\text{TP}_r + \text{FN}_r}, \quad (4)$$

where TP_r , FP_r , and FN_r denote true positives, false positives, and false negatives within a regional tolerance radius r . The AuPRC_r is computed as Eq. (5):

$$\text{AuPRC}_r = \int_0^1 \text{Precision}_r(\text{Recall}_r) d(\text{Recall}_r). \quad (5)$$

4. OccOoD: Proposed Framework

4.1. Problem Setting

Out-of-distribution segmentation in 2D pinhole images typically relies on pixel-wise classification scores. Building on this concept, we extend out-of-distribution detection to 3D semantic occupancy prediction at the voxel level. Given an input image $I \in \mathbb{R}^{C \times H \times W}$, the semantic occupancy prediction process yields a volumetric representation $V \in \mathbb{R}^{C \times H \times W \times Z}$, where Z denotes the depth dimension. The voxel-level classification scores $Q(V) \in \mathbb{R}^{K \times H \times W \times Z}$ are then obtained. To assess anomalies at the voxel level, an anomaly score $A(V) \in \mathbb{R}^{H \times W \times Z}$ is computed as Eq. (6):

$$A(V) = f(Q(V)), \quad (6)$$

where K denotes the number of classes for the semantic prediction, C , H , W , and Z correspond to the channels, height, width, and depth of the voxel space, respectively.

4.2. Overall Architecture

The OccOoD framework, illustrated in Fig. 4, integrates front-view and BEV representations for precise 3D semantic occupancy prediction. While 3D voxels preserve fine-grained geometric details, BEV enhances spatial reasoning and global scene understanding. To effectively merge these representations, we propose Voxel-BEV Progressive Fusion (VBPF), which iteratively refines voxel-BEV integration, leveraging voxel geometry and BEV efficiency for

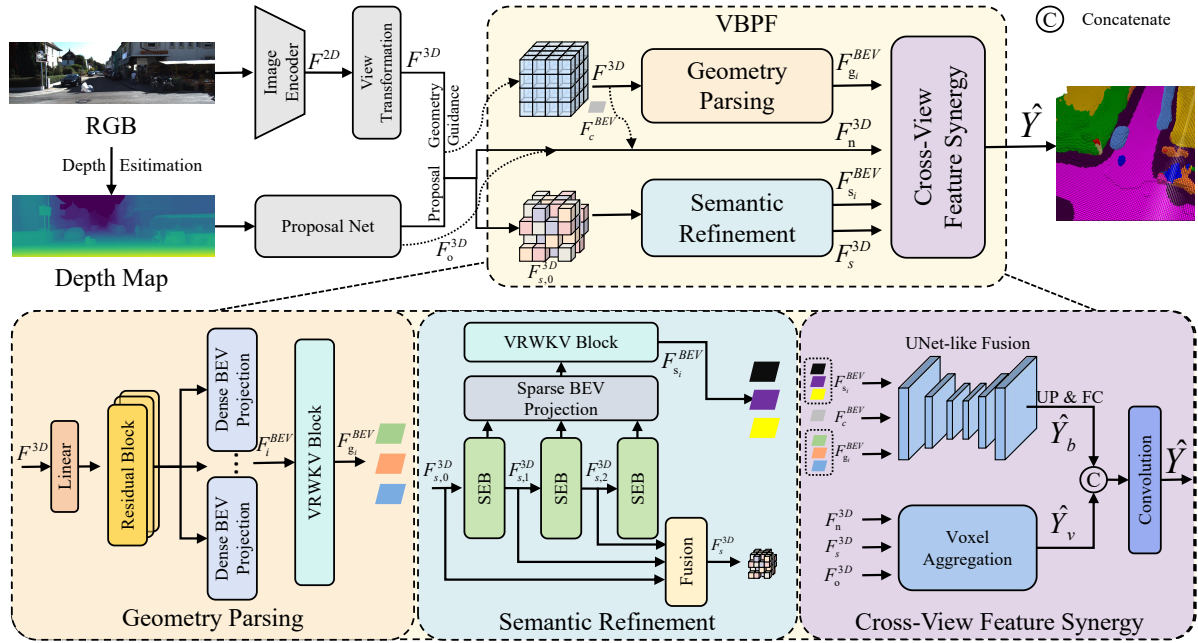


Figure 4. An overview of the proposed OccOoD framework. The image encoder extracts 2D features and converts them into 3D features via View Transformation, guided by geometric occupancy. Seed voxels and other features are processed through geometry parsing and semantic refinement to generate enhanced BEV and voxel features. Finally, cross-view feature synergy integrates these representations for rich geometry and high spatial efficiency.

improved feature representation. This multi-perspective fusion enhances generalization and robustness, significantly boosting out-of-distribution detection performance. Initially, following SGN [66], an image encoder extracts 2D features from RGB images, which are then mapped into 3D space using a view transformation module adapted from MonoScene [12]. The coarse 3D features are refined through geometry guidance, and an auxiliary 3D occupancy head is optimized using binary cross-entropy loss:

$$L_{\text{geo}} = - \sum_i \left[(1 - Y_{o,i}) \log(1 - \hat{Y}_{o,i}) + Y_{o,i} \log(\hat{Y}_{o,i}) \right], \quad (7)$$

where i indexes voxels, Y_o represents ground truth occupancy, and \hat{Y}_o indicates the predicted occupancy.

After the proposal network filters the 3D features, optimized with a binary cross-entropy loss L_{occ} , the filtered features undergo Geometry Parsing and Semantic Refinement to extract multi-scale BEV features and fine-grained semantic voxel features. These BEV features are fused with the original 3D features through a UNet-like module, ensuring precise alignment and enhanced representation learning. Finally, the BEV representation is upsampled, concatenated with the aggregated voxel representation, and refined using convolutions to produce the semantic occupancy prediction.

4.3. Voxel-BEV Progressive Fusion

The coarse voxel features F^{3D} from the view transformation module and the seed features $F_{s,0}^{3D}$ obtained through the

proposal network are both 3D voxel features. However, a single representation limits fine-grained semantics and segmentation boundaries, hindering OoD detection. To overcome this, VBPF progressively integrates voxel-based and BEV representations, leveraging BEV’s top-down perspective for global context and spatial uncertainty identification.

Geometry Parsing: The coarse voxel features F^{3D} are processed through a geometric parsing branch, comprising a linear layer, residual connections, a BEV projection module, and a Vision-RWKV (VRWKV) module [26] (see Fig. 4), to encode rich geometric information into compact BEV representations.

Specifically, F^{3D} is initially projected into a lower-dimensional space via a linear layer, refined through a residual block, aligned along the z-axis, and compressed using 2D convolutions to generate dense BEV features. These BEV features are further refined by the VRWKV module, which enhances their representational quality through spatial and channel mixing operations, producing dense geometric BEV features $\{F_i^{\text{BEV}}\}_i$.

Semantic Refinement: The seed voxels $F_{s,0}^{3D}$ generated by the proposal network undergo semantic refinement to enhance semantic accuracy. The semantic refinement module comprises three cascaded sparse encoder blocks (SEB), each linked with a BEV projection module and a VRWKV block. Each SEB contains a Sparse Feature Encoder (SFE) [107] and a Sparse Geometry Feature Encoder

(SGFE) [107], which optimize the initial semantic representation and refine it through hierarchical pooling and attention mechanisms, capturing fine-grained local details and broader contextual dependencies.

First, the voxel features pass through the SEB, where two SEBs output contextual features at different scales, $F_{s,1}^{3D}$ and $F_{s,2}^{3D}$, each embedding rich geometric and contextual information. These features are projected into BEV space via a BEV projection operation, where max-pooling aggregates features with the same BEV index, generating sparse BEV features, which are then converted into dense semantic-BEV features using Sponcv’s densification function.

The VRWKV module is then applied to model long-range dependencies, enhancing the representational quality of the BEV features. The final output includes multi-scale semantic BEV features: $\{F_{s_i}^{\text{BEV}}\}_i$, as well as the refined semantic feature F_s^{3D} obtained by Eq. (8):

$$F_s^{3D} = \text{MLP}([F_{s,0}^{3D}, F_{s,1}^{3D}, F_{s,2}^{3D}]). \quad (8)$$

The multi-scale semantic BEV features $\{F_{s_i}^{\text{BEV}}\}_i$ are used for BEV-level fusion, while the refined semantic feature F_s^{3D} is utilized for voxel-level fusion. Additionally, F_s^{3D} is passed through an auxiliary semantic head (a two-layer MLP) to predict the corresponding semantics \hat{Y}_s .

The semantic refinement stage is optimized using a combination of cross-entropy loss and Lovasz loss [6]:

$$L_{sem} = L_{ce}(\hat{Y}_s, Y_s) + L_{lovasz}(\hat{Y}_s, Y_s), \quad (9)$$

where Y_s represents the semantic labels of seed voxels indexed from the semantic scene labels Y .

Cross-View Feature Synergy: To effectively integrate BEV and voxel-level representations, we first extract features independently. For BEV processing, we employ a UNet-like architecture, where the encoder captures hierarchical spatial features and the decoder reconstructs high-resolution feature maps for seamless fusion. The inputs include the projection of 3D features into BEV space (F_c^{BEV}), geometric BEV features $\{F_g^{\text{BEV}}\}_i$ from the first stage, and semantic BEV features $\{F_{s_i}^{\text{BEV}}\}_i$ from the second stage.

The BEV encoder downsamples F_c^{BEV} through convolutional blocks, each followed by a VRWKV block, and integrates geometric BEV features F_g^{BEV} and semantic BEV features $F_{s_i}^{\text{BEV}}$ using an ARF module [65]. The process can be represented as Eq. (10):

$$F_{f_i}^{\text{BEV}} = \sum_{k \in \{g, s, c\}} (F_{k_i}^{\text{BEV}} \odot A_{k_i}^{\text{BEV}}), \quad (10)$$

where $F_{k_i}^{\text{BEV}}$ and $A_{k_i}^{\text{BEV}}$ represent the k -th class feature map of the i -th BEV feature and its corresponding attention weight, respectively. The decoder restores spatial resolution using transposed convolutions and skip connections.

The processed BEV features are reshaped and upsampled to generate a voxel-level representation \hat{Y}_b .

For voxel-level feature processing, we adopt the approach of SGN [66] for voxel handling. Specifically, we fuse and refine three types of features: F_s^{3D} obtained from semantic refinement, non-seed voxel features F_n^{3D} filtered by the proposal network, and F_o^{3D} from the proposal network. This procedure is formally expressed in Eq. (11):

$$\hat{Y}_v = \text{MSSP}([F_s^{3D}, F_n^{3D}, F_o^{3D}]), \quad (11)$$

where MSSP denotes the multi-scale semantic propagation.

Subsequently, \hat{Y}_v is concatenated with \hat{Y}_b and processed through a 1D convolutional layer to generate the final unified representation \hat{Y}_f . We optimize the model using a combination of scene- and class-wise semantic loss L_{sem}^{scal} , geometry L_{geo}^{scal} , and cross-entropy loss L_{ce} . The overall loss function is defined in Eq. (12):

$$L_{ssc} = L_{sem}^{scal}(\hat{Y}, Y) + L_{geo}^{scal}(\hat{Y}, Y) + L_{ce}(\hat{Y}, Y), \quad (12)$$

where L_{sem}^{scal} ensures semantic consistency at both scene and class levels, L_{geo}^{scal} enforces geometric fidelity, and L_{ce} minimizes classification errors.

Loss Function: The total training loss is defined as follows:

$$L = L_{geo} + L_{occ} + L_{sem} + L_{ssc}. \quad (13)$$

4.4. OoD Occupancy Prediction

After achieving high-precision semantic occupancy prediction, we further integrate an out-of-distribution detection mechanism to identify outliers that deviate from the in-distribution regions. For the semantic occupancy prediction results \hat{Y}_f , we compute the category-specific anomaly score $A(V)$ for each voxel according to the predictive semantics.

Geometry Prior: To more efficiently focus on non-empty regions, we introduce a geometry prior by applying an *argmax* operation to \hat{Y}_f . This strategy prioritizes potentially anomalous non-empty regions, significantly improving the effectiveness and accuracy of OoD detection.

Semantic-aware Anomaly Scoring: We categorize voxels into two groups based on their semantic predictions: **instance** (e.g., *car*, *person*, *bicycle*), and **region** (e.g., *road*, *sidewalk*, *vegetation*). Anomaly scores are computed using methods tailored to each group’s unique characteristics.

- For **instance**, we employ *cosine similarity* to measure deviations in feature space, as these classes often exhibit distinct geometric and semantic features. The cosine similarity for per-voxel’s logit is computed as:

$$S_{\cosine}(v_i) = 1 - \cos(\mathbf{l}(v_i), \bar{\mathbf{l}}), \quad (14)$$

where $\mathbf{l}(v_i)$ is the logit vector of voxel v_i , and $\bar{\mathbf{l}}$ is the mean logit vector of the same class.

Methods	VAA-KITTI				VAA-KITTI-360			
	AuPRC _r ↑			AuROC↑	AuPRC _r ↑			AuROC↑
	0.8m	1.0m	1.2m		0.8m	1.0m	1.2m	
SGN-S [66]	16.00	24.08	35.09	65.99	17.42	19.99	23.51	66.31
OccOoD-S (ours)	19.64	27.75	38.69	65.91	22.89	25.59	29.21	67.34

Table 1. Quantitative results across different region ranges on the VAA-KITTI and VAA-KITTI-360 datasets. The best results are in **bold**.

Method	IoU	road	sidewalk	parking	other-gmd.	building	car	truck	bicycle	motorcycle	other-veh.	vegetation	trunk	terrain	person	bicyclist	motorcyclist	fence	pole	traf.-sign	mIoU
		■	■	■	■	■	■	■	■	■	■	■	■	■	■	■	■	■	■	■	
SemanticKITTI																					
VoxFormer [51]	43.21	54.10	26.90	25.10	7.30	23.50	21.70	3.60	1.90	<u>1.60</u>	4.10	24.40	8.10	24.20	1.60	<u>1.10</u>	0.00	13.10	6.60	5.70	13.41
SGN [66]	45.42	60.40	31.40	28.90	8.70	28.40	25.40	4.50	0.90	<u>1.60</u>	3.70	27.40	12.60	28.40	0.50	0.30	0.10	18.10	10.00	<u>8.30</u>	15.76
Symphonies [41]	42.19	58.40	29.30	26.90	<u>11.70</u>	24.70	23.60	3.20	<u>3.60</u>	2.60	5.60	24.20	10.00	23.10	3.20	1.90	2.00	16.10	7.70	8.00	15.04
CGFormer [110]	44.41	64.30	34.20	34.10	12.10	25.80	<u>26.10</u>	<u>4.30</u>	3.70	1.30	2.70	24.50	11.20	29.30	<u>1.70</u>	3.60	<u>0.40</u>	18.70	8.70	9.30	16.63
OccOoD (Ours)	<u>45.11</u>	<u>61.80</u>	<u>31.60</u>	<u>30.50</u>	10.00	<u>27.90</u>	26.60	2.60	1.00	0.80	5.60	<u>26.70</u>	<u>11.90</u>	<u>28.90</u>	0.50	0.80	0.00	18.70	<u>9.40</u>	5.70	<u>15.85</u>
VAA-KITTI																					
SGN-S [66]	39.07	46.62	26.54	15.88	0.12	18.34	20.51	0.62	0.44	0.35	1.23	24.76	6.40	21.78	0.48	1.29	0.00	12.25	8.70	4.57	11.10
OccOoD-S (Ours)	40.04	50.17	27.42	18.4	0.01	17.38	20.19	0.74	0.26	0.56	1.04	25.13	5.53	23.56	0.67	1.95	0.00	11.35	8.15	5.80	11.49

Table 2. Quantitative results on the SemanticKITTI test set [3] and VAA-KITTI. The best and the second best results are in **bold** and underlined, respectively.

- For **region**, we use *entropy-based scoring* to capture prediction uncertainty, as these classes typically cover larger, more homogeneous areas. The entropy-based anomaly score is computed as:

$$S_{\text{entropy}}(v_i) = - \sum_{k \in \mathcal{K}} p(k|v_i) \log p(k|v_i), \quad (15)$$

where \mathcal{K} represents the set of possible classes, and $p(k|v_i)$ denotes the probability that voxel v_i is predicted to be of class k . To prioritize instance classes, the anomaly scores for region classes are weighted accordingly. Higher entropy values indicate greater uncertainty, which is often associated with OoD regions.

Ultimately, the anomaly scores $A(V)$ are normalized to $[0, 1]$ to ensure comparability across classes. Voxels predicted as empty are assigned the minimum anomaly score, effectively filtering them from further analysis.

5. Experiments

Two sets of experiments are conducted to evaluate the effectiveness of the proposed OccOoD framework. First, we assessed its performance on OoD on established datasets. Then, we evaluated the performance of semantic occupancy prediction on public benchmarks as well as established datasets. After that, we performed several ablation studies to validate the effectiveness of our design. For additional details on datasets, evaluation metrics, and implementation specifics, please refer to the supplementary materials.

5.1. Results on Different Datasets

Quantitative Results: In Table 1, the OoD detection results are reported. Across the three different scales of AuPRC_r, our network achieves a significant improvement over the baseline. On the VAA-KITTI dataset, our performance improves by more than 3% in terms of AuPRC_r. Similarly, on the VAA-KITTI-360 dataset, our method demonstrates a performance gain of over 5%. Furthermore, we present the experimental results of semantic occupancy prediction in Table 2. Our method consistently demonstrates performance improvements over the baseline model, regardless of whether the evaluation is conducted on public datasets or our self-constructed datasets. These results fully validate the effectiveness of our designed VBPF, which progressively integrates features from the BEV perspective, thereby enhancing global context perception. For more details on experimental results, please refer to the supplementary materials.

Qualitative Results: In Fig. 5, four different sets of visualization results are presented. It can be observed that without incorporating a top-down perspective, the baseline network exhibits significant estimation biases. Specifically, by integrating two different observation perspectives, our network achieves more accurate localization for small objects (skunk). Meanwhile, for elongated objects (cow), accurately determining their size from a single image alone is inherently challenging. However, by leveraging multi-view observations, the proposed network makes predictions that

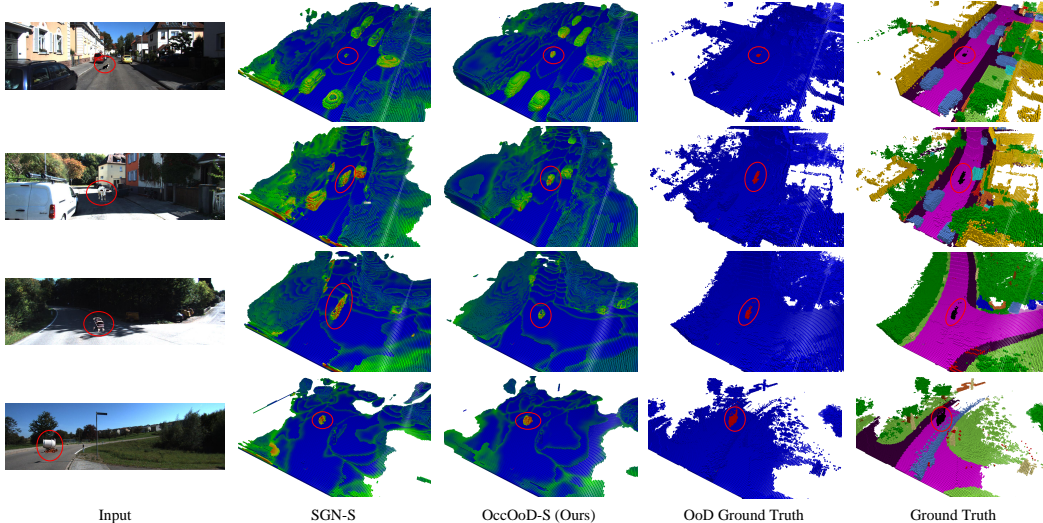


Figure 5. Visualization of the results on the VAA-KITTI. From left to right are the input RGB images, the SGN-S [66] results, the OccOoD-S (ours) results, the OoD ground truths, and the semantic occupancy prediction ground truths. Zoom in for a better view.

Anomaly Score Methods	VAA-KITTI			VAA-KITTI-360				
	AuPRC _r ↑ 0.8m	AuPRC _r ↑ 1.0m	AuPRC _r ↑ 1.2m	AuROC↑	AuPRC _r ↑ 0.8m	AuPRC _r ↑ 1.0m	AuPRC _r ↑ 1.2m	AuROC↑
Entropy	7.99	14.14	23.38	63.84	7.44	10.26	14.11	65.51
Postpro	6.61	11.53	18.83	64.43	7.86	10.93	13.69	65.25
Energy	8.02	14.12	23.26	62.79	7.40	10.24	14.14	63.20
ASS (Ours)	19.64	27.75	38.69	65.91	22.89	25.59	29.21	67.34

Table 3. Ablation studies of OccOoD on established datasets.

Methods	VAA-KITTI		VAA-KITTI-360	
	AuPRC _r ↑	AuROC↑	AuPRC _r ↑	AuROC↑
w/o Geometry prior	17.42	75.60	11.14	73.52
Geometry prior	38.69	65.91	29.21	67.34

Table 4. Ablation and comparison studies of geometry prior on established datasets and regions within 1.2m.

are more physically consistent and geometrically plausible.

5.2. Ablation Studies

Semantic-aware Anomaly Scoring: Table 3 demonstrates the effectiveness of our proposed Semantic-aware Anomaly Scoring (ASS). Compared to the other three scoring methods, our approach improves AuPRC_r by more than 10% across all scales. This is because we incorporate the spatial occupancy characteristics of different objects in 3D space, applying a cosine similarity method for instance-level objects while using an entropy-based approach for larger and more uniform regions. Moreover, in terms of AuROC, we also achieved impressive improvements.

Geometry Prior: In Table 4, we analyze the importance of Geometry Prior by examining AuPRC_r and AuROC. With the geometry prior, the network achieves a significant improvement in AuPRC_r. In the absence of the geometry prior, the higher AuROC score is due to the fact that it also considers the uncertainty of empty voxel as an anomaly voxel. In our dataset, positive samples are extremely rare,

making the AuPRC_r metric more suitable for evaluating the model’s performance.

Sequences Used for Training				Depth Estimation Model Used for Training			
Methods	#Sequences	IoU	mIoU	Methods	Depth Estimation Model	IoU	mIoU
SGN-T [66]	10	46.21	15.32	SGN-S [66]	MobileStereoNet [76]	42.76	14.06
OccOoD-T		46.83	16.80	OccOoD-S		43.33	14.54
SGN-T [66]	7	45.15	15.23	SGN-S [66]	SPI [45]	41.65	13.68
OccOoD-T		45.49	15.86	OccOoD-S		42.75	13.79

Table 5. Ablation and comparison studies on SemanticKITTI val set [3]. The left table examines different training sequences, whereas the right table studies different depth estimation models.

Impact of Depth Prior: Table 5 demonstrates the impact of different depth models on detection performance. Using only monocular depth estimation, our method outperforms the baseline by 1.1%. With the more accurate MSNet3D model [76], the improvement reaches 0.57%. The top-down observation perspective mitigates depth map limitations, enabling our network with monocular depth to nearly match the baseline’s performance using stereo-depth maps.

6. Conclusion

In this study, we look into out-of-distribution semantic occupancy prediction to address OoD voxel detection in 3D space. To address the scarcity of anomaly annotations in existing datasets, we developed a Synthetic Anomaly Integration Pipeline and introduced two datasets, VAA-KITTI and VAA-KITTI-360, for evaluating OoD detection in 3D occupancy tasks. We put forward OccOoD to integrate OoD detection into 3D semantic occupancy prediction. By combining voxel-based and BEV representations, OccOoD effectively captures both local details and global context, thereby enhancing its semantic and geometric understanding. Experiments show that OccOoD delivers state-of-the-art OoD detection performance on VAA-KITTI and VAA-

KITTI-360, while also maintaining competitive occupancy prediction performance on public benchmarks.

Limitation: The performance of current semantic occupancy prediction methods is limited by geometric inaccuracies in estimated occupancy grids, which adversely affect precision of anomaly detection. We anticipate that future advancements in the field will substantially address these limitations, leading to more robust 3D perception.

Acknowledgment

This work was supported in part by the National Natural Science Foundation of China (No. 62473139) and in part by the Open Research Project of the State Key Laboratory of Industrial Control Technology, China (Grant No. ICT2025B20).

References

- [1] Jan Ackermann, Christos Sakaridis, and Fisher Yu. Maskomaly: Zero-shot mask anomaly segmentation. In *BMVC*, 2023. 2
- [2] Mariette Awad, Rahul Khanna, Mariette Awad, and Rahul Khanna. Support vector regression. *Efficient Learning Machines: Theories, Concepts, and Applications for Engineers and System Designers*, 2015. 3
- [3] Jens Behley, Martin Garbade, Andres Milioto, Jan Quenzel, Sven Behnke, Cyrill Stachniss, and Jurgen Gall. SemanticKITTI: A dataset for semantic scene understanding of LiDAR sequences. In *ICCV*, 2019. 2, 4, 7, 8, 14, 15, 16
- [4] Paul Bergmann and David Sattlegger. Anomaly detection in 3D point clouds using deep geometric descriptors. In *WACV*, 2023. 2
- [5] Paul Bergmann, Xin Jin, David Sattlegger, and Carsten Steger. The MVTec 3D-AD dataset for unsupervised 3D anomaly detection and localization. In *VISAPP*, 2022. 2
- [6] Maxim Berman, Amal Rannen Triki, and Matthew B. Blaschko. The Lovász-Softmax loss: A tractable surrogate for the optimization of the intersection-over-union measure in neural networks. In *CVPR*, 2018. 6
- [7] Ankan Bhunia, Changjian Li, and Hakan Bilen. Looking 3D: Anomaly detection with 2D-3D alignment. In *CVPR*, 2024. 2
- [8] Hermann Blum, Paul-Edouard Sarlin, Juan Nieto, Roland Siegwart, and Cesar Cadena. The fishyscapes benchmark: Measuring blind spots in semantic segmentation. *International Journal of Computer Vision*, 2021. 1, 2, 15
- [9] Simon Boeder, Fabian Gigengack, and Benjamin Risse. LangOcc: Self-supervised open vocabulary occupancy estimation via volume rendering. *arXiv preprint arXiv:2407.17310*, 2024. 2
- [10] Simon Boeder, Fabian Gigengack, and Benjamin Risse. OccFlowNet: Towards self-supervised occupancy estimation via differentiable rendering and occupancy flow. *arXiv preprint arXiv:2402.12792*, 2024. 2
- [11] Simon Boeder, Fabian Gigengack, and Benjamin Risse. GaussianFlowOcc: Sparse and weakly supervised occupancy estimation using gaussian splatting and temporal flow. *arXiv preprint arXiv:2502.17288*, 2025. 2
- [12] Anh-Quan Cao and Raoul De Charette. MonoScene: Monocular 3D semantic scene completion. In *CVPR*, 2022. 1, 5, 16
- [13] Anh-Quan Cao, Angela Dai, and Raoul De Charette. PaSCo: Urban 3D panoptic scene completion with uncertainty awareness. In *CVPR*, 2024. 2
- [14] Helin Cao and Sven Behnke. SLCF-Net: Sequential LiDAR-camera fusion for semantic scene completion using a 3D recurrent U-Net. In *ICRA*, 2024. 2
- [15] Yunkang Cao, Xiaohao Xu, and Weiming Shen. Complementary pseudo multimodal feature for point cloud anomaly detection. *Pattern Recognition*, 2024. 2
- [16] Jun Cen, Peng Yun, Junhao Cai, Michael Yu Wang, and Ming Liu. Deep metric learning for open world semantic segmentation. In *ICCV*, 2021. 2
- [17] Robin Chan, Krzysztof Lis, Svenja Uhlemeyer, Hermann Blum, Sina Honari, Roland Siegwart, Pascal Fua, Mathieu Salzmann, and Matthias Rottmann. SegmentMelfYouCan: A benchmark for anomaly segmentation. In *NeurIPS*, 2021. 1, 2, 15
- [18] Robin Chan, Matthias Rottmann, and Hanno Gottschalk. Entropy maximization and meta classification for out-of-distribution detection in semantic segmentation. In *ICCV*, 2021. 2
- [19] Ran Cheng, Christopher Agia, Yuan Ren, Xinhai Li, and Liu Bingbing. S3CNet: A sparse semantic scene completion network for LiDAR point clouds. In *CoRL*, 2021. 2
- [20] Hyunjun Choi, Hawook Jeong, and Jin Young Choi. Balanced energy regularization loss for out-of-distribution detection. In *CVPR*, 2023. 2
- [21] Charles Corbière, Nicolas Thome, Avner Bar-Hen, Matthieu Cord, and Patrick Pérez. Addressing failure prediction by learning model confidence. In *NeurIPS*, 2019. 2
- [22] Marius Cordts, Mohamed Omran, Sebastian Ramos, Timo Rehfeld, Markus Enzweiler, Rodrigo Benenson, Uwe Franke, Stefan Roth, and Bernt Schiele. The cityscapes dataset for semantic urban scene understanding. In *CVPR*, 2016. 2
- [23] Yubo Cui, Zhiheng Li, Jiaqiang Wang, and Zheng Fang. LOMA: Language-assisted semantic occupancy network via triplane mamba. In *AAAI*, 2025. 2
- [24] Pau de Jorge, Riccardo Volpi, Puneet K. Dokania, Philip H. S. Torr, and Grégory Rogez. Placing objects in context via inpainting for out-of-distribution segmentation. In *ECCV*, 2024. 3
- [25] Anja Delic, Matej Grcic, and Sinisa Segvic. Outlier detection by ensembling uncertainty with negative objectness. In *BMVC*, 2024. 2
- [26] Yuchen Duan, Weiyun Wang, Zhe Chen, Xizhou Zhu, Lewei Lu, Tong Lu, Yu Qiao, Hongsheng Li, Jifeng Dai, and Wenhai Wang. Vision-RWKV: Efficient and scalable visual perception with RWKV-like architectures. *arXiv preprint arXiv:2403.02308*, 2024. 5, 14

- [27] Matej Grcic, Petra Bevandic, Zoran Kalafatic, and Sinisa Segvic. Dense anomaly detection by robust learning on synthetic negative data. *arXiv preprint arXiv:2112.12833*, 2021. 2
- [28] Matej Grcic, Petra Bevandic, and Sinisa Segvic. DenseHybrid: Hybrid anomaly detection for dense open-set recognition. In *ECCV*, 2022. 2
- [29] Matej Grcic, Josip Saric, and Sinisa Segvic. On advantages of mask-level recognition for outlier-aware segmentation. In *CVPRW*, 2023. 2
- [30] Shangwei Guo, Hao Shi, Song Wang, Xiaoting Yin, Kailun Yang, and Kaiwei Wang. Event-aided semantic scene completion. *arXiv preprint arXiv:2502.02334*, 2025. 2
- [31] David Haldimann, Hermann Blum, Roland Siegwart, and Cesar Cadena. This is not what I imagined: Error detection for semantic segmentation through visual dissimilarity. *arXiv preprint arXiv:1909.00676*, 2019. 2
- [32] Adrian Hayler, Felix Wimbauer, Dominik Muhle, Christian Rupprecht, and Daniel Cremers. S4C: Self-supervised semantic scene completion with neural fields. In *3DV*, 2024. 2
- [33] Dan Hendrycks, Steven Basart, Mantas Mazeika, Andy Zou, Joseph Kwon, Mohammadreza Mostajabi, Jacob Steinhardt, and Dawn Song. Scaling out-of-distribution detection for real-world settings. *arXiv preprint arXiv:1911.11132*, 2019. 1, 2, 15
- [34] Eliahu Horwitz and Yedid Hoshen. Back to the feature: Classical 3D features are (almost) all you need for 3D anomaly detection. In *CVPR*, 2023. 2
- [35] Jiawei Hou, Xiaoyan Li, Wenhao Guan, Gang Zhang, Di Feng, Yuheng Du, Xiangyang Xue, and Jian Pu. FastOcc: Accelerating 3D occupancy prediction by fusing the 2D bird’s-eye view and perspective view. In *ICRA*, 2024. 2
- [36] Yihan Hu, Jiazhi Yang, Li Chen, Keyu Li, Chonghao Sima, Xizhou Zhu, Siqi Chai, Senyao Du, Tianwei Lin, Wenhao Wang, Lewei Lu, Xiaosong Jia, Qiang Liu, Jifeng Dai, Yu Qiao, and Hongyang Li. Planning-oriented autonomous driving. In *CVPR*, 2023. 1
- [37] Yuanhui Huang, Wenzhao Zheng, Yunpeng Zhang, Jie Zhou, and Jiwen Lu. Tri-perspective view for vision-based 3D semantic occupancy prediction. In *CVPR*, 2023. 1, 16
- [38] Yuanhui Huang, Wenzhao Zheng, Borui Zhang, Jie Zhou, and Jiwen Lu. SelfOcc: Self-supervised vision-based 3D occupancy prediction. In *CVPR*, 2024. 2
- [39] Yuanhui Huang, Wenzhao Zheng, Yunpeng Zhang, Jie Zhou, and Jiwen Lu. GaussianFormer: Scene as gaussians for vision-based 3D semantic occupancy prediction. In *ECCV*, 2024. 2
- [40] Hyun-Kurl Jang, Jihun Kim, Hyeokjun Kweon, and Kuk-Jin Yoon. TALoS: Enhancing semantic scene completion via test-time adaptation on the line of sight. In *NeurIPS*, 2024. 2
- [41] Haoyi Jiang, Tianheng Cheng, Naiyu Gao, Haoyang Zhang, Tianwei Lin, Wenyu Liu, and Xinggang Wang. Symphonize 3D semantic scene completion with contextual instance queries. In *CVPR*, 2024. 1, 2, 7, 15, 16
- [42] Haoyi Jiang, Liu Liu, Tianheng Cheng, Xinjie Wang, Tianwei Lin, Zhizhong Su, Wenyu Liu, and Xinggang Wang. GaussTR: Foundation model-aligned gaussian transformer for self-supervised 3D spatial understanding. In *CVPR*, 2025. 2
- [43] Sanghun Jung, Jungsoo Lee, Daehoon Gwak, Sungha Choi, and Jaegul Choo. Standardized max logits: A simple yet effective approach for identifying unexpected road obstacles in urban-scene segmentation. In *ICCV*, 2021. 2
- [44] Jungho Kim, Changwon Kang, Dongyoung Lee, Sehwan Choi, and Jun Won Choi. ProtoOcc: Accurate, efficient 3D occupancy prediction using dual branch encoder-prototype query decoder. In *AAAI*, 2025. 2
- [45] Mykola Lavreniuk. SPIdepth: Strengthened pose information for self-supervised monocular depth estimation. *arXiv preprint arXiv:2404.12501*, 2024. 8
- [46] Bohan Li, Jiajun Deng, Wenyao Zhang, Zhuji Liang, Dalong Du, Xin Jin, and Wenjun Zeng. Hierarchical temporal context learning for camera-based semantic scene completion. In *ECCV*, 2024. 2
- [47] Heng Li, Yuenan Hou, Xiaohan Xing, Xiao Sun, and Yanyong Zhang. OccMamba: Semantic occupancy prediction with state space models. *arXiv preprint arXiv:2408.09859*, 2024. 2
- [48] Jinke Li, Xiao He, Chonghua Zhou, Xiaoqiang Cheng, Yang Wen, and Dan Zhang. ViewFormer: Exploring spatiotemporal modeling for multi-view 3D occupancy perception via view-guided transformers. In *ECCV*, 2024. 2
- [49] Jianing Li, Ming Lu, Hao Wang, Chenyang Gu, Wenzhao Zheng, Li Du, and Shanghang Zhang. SliceOcc: Indoor 3D semantic occupancy prediction with vertical slice representation. In *ICRA*, 2025. 2
- [50] Wenqiao Li, Xiaohao Xu, Yao Gu, Bozhong Zheng, Shenghua Gao, and Yingna Wu. Towards scalable 3D anomaly detection and localization: A benchmark via 3D anomaly synthesis and a self-supervised learning network. In *CVPR*, 2024. 2
- [51] Yiming Li, Zhiding Yu, Christopher B. Choy, Chaowei Xiao, José M. Álvarez, Sanja Fidler, Chen Feng, and Anima Anandkumar. VoxFormer: Sparse voxel transformer for camera-based 3D semantic scene completion. In *CVPR*, 2023. 1, 2, 7, 15, 16
- [52] Yiming Li, Sihang Li, Xinhao Liu, Moonjun Gong, Kenan Li, Nuo Chen, Zijun Wang, Zhiheng Li, Tao Jiang, Fisher Yu, Yue Wang, Hang Zhao, Zhiding Yu, and Chen Feng. SSCBench: A large-scale 3D semantic scene completion benchmark for autonomous driving. In *IROS*, 2024. 2, 4, 14, 15
- [53] Zhiqi Li, Wenhao Wang, Hongyang Li, Enze Xie, Chonghao Sima, Tong Lu, Yu Qiao, and Jifeng Dai. BEVFormer: Learning bird’s-eye-view representation from multi-camera images via spatiotemporal transformers. In *ECCV*, 2022. 1
- [54] Li Liang, Naveed Akhtar, Jordan Vice, Xiangrui Kong, and Ajmal Saeed Mian. Skip mamba diffusion for monocular 3D semantic scene completion. In *AAAI*, 2025. 2
- [55] Krzysztof Lis, Krishna Nakka, Pascal Fua, and Mathieu Salzmann. Detecting the unexpected via image resynthesis. In *ICCV*, 2019. 1, 2, 15

- [56] Haisong Liu, Yang Chen, Haiguang Wang, Zetong Yang, Tianyu Li, Jia Zeng, Li Chen, Hongyang Li, and Limin Wang. Fully sparse 3D occupancy prediction. In *ECCV*, 2024. 2
- [57] Jiaqi Liu, Guoyang Xie, Ruitao Chen, Xinpeng Li, Jinbao Wang, Yong Liu, Chengjie Wang, and Feng Zheng. Real3D-AD: A dataset of point cloud anomaly detection. In *NeurIPS*, 2023. 2
- [58] Yuyuan Liu, Choubo Ding, Yu Tian, Guansong Pang, Vasileios Belagiannis, Ian Reid, and Gustavo Carneiro. Residual pattern learning for pixel-wise out-of-distribution detection in semantic segmentation. In *ICCV*, 2023. 2
- [59] Thibaut Loiseau, Tuan-Hung Vu, Mickael Chen, Patrick Pérez, and Matthieu Cord. Reliability in semantic segmentation: Can we use synthetic data? In *ECCV*, 2024. 3
- [60] Ilya Loshchilov and Frank Hutter. Decoupled weight decay regularization. In *ICLR*, 2019. 14
- [61] Yuhang Lu, Xinge Zhu, Tai Wang, and Yuexin Ma. OctreeOcc: Efficient and multi-granularity occupancy prediction using octree queries. In *NeurIPS*, 2024. 2
- [62] Qihang Ma, Xin Tan, Yanyun Qu, Lizhuang Ma, Zhizhong Zhang, and Yuan Xie. COTR: Compact occupancy transformer for vision-based 3D occupancy prediction. In *CVPR*, 2024. 1, 2
- [63] Tao Ma, Hongbin Zhou, Qiusheng Huang, Xuemeng Yang, Jianfei Guo, Bo Zhang, Min Dou, Yu Qiao, Botian Shi, and Hongsheng Li. ZOPP: A framework of zero-shot offboard panoptic perception for autonomous driving. In *NeurIPS*, 2024. 2
- [64] Yukai Ma, Jianbiao Mei, Xuemeng Yang, Licheng Wen, Weihua Xu, Jiangning Zhang, Xingxing Zuo, Botian Shi, and Yong Liu. LiCROcc: Teach radar for accurate semantic occupancy prediction using LiDAR and camera. *IEEE Robotics and Automation Letters*, 2024. 2
- [65] Jianbiao Mei, Yu Yang, Mengmeng Wang, Tianxin Huang, Xuemeng Yang, and Yong Liu. SSC-RS: Elevate LiDAR semantic scene completion with representation separation and BEV fusion. In *IROS*, 2023. 6, 14
- [66] Jianbiao Mei, Yu Yang, Mengmeng Wang, Junyu Zhu, Jongwon Ra, Yukai Ma, Laijian Li, and Yong Liu. Camera-based 3D semantic scene completion with sparse guidance network. *IEEE Transactions on Image Processing*, 2024. 1, 2, 5, 6, 7, 8, 14, 15, 16
- [67] Jishnu Mukhoti and Yarín Gal. Evaluating bayesian deep learning methods for semantic segmentation. *arXiv preprint arXiv:1811.12709*, 2018. 2
- [68] Nazir Nayal, Misra Yavuz, João F. Henriques, and Fatma Güney. RbA: Segmenting unknown regions rejected by all. In *ICCV*, 2023. 2
- [69] Wenzhe Ouyang, Zenglin Xu, Bin Shen, Jinghua Wang, and Yong Xu. LinkOcc: 3D semantic occupancy prediction with temporal association. *IEEE Transactions on Circuits and Systems for Video Technology*, 2024. 2
- [70] Jingyi Pan, Zipeng Wang, and Lin Wang. Co-Occ: Coupling explicit feature fusion with volume rendering regularization for multi-modal 3D semantic occupancy prediction. *IEEE Robotics and Automation Letters*, 2024. 2
- [71] Mingjie Pan, Jiaming Liu, Renrui Zhang, Peixiang Huang, Xiaoqi Li, Hongwei Xie, Bing Wang, Li Liu, and Shanghang Zhang. RenderOcc: Vision-centric 3D occupancy prediction with 2D rendering supervision. In *ICRA*, 2024. 2
- [72] Yancheng Pan, Biao Gao, Jilin Mei, Sibao Geng, Chengkun Li, and Huijing Zhao. SemanticPOSS: A point cloud dataset with large quantity of dynamic instances. In *IV*, 2020. 15
- [73] Kunyu Peng, Juncong Fei, Kailun Yang, Alina Roitberg, Jiaming Zhang, Frank Bieder, Philipp Heidenreich, Christoph Stiller, and Rainer Stiefelhagen. MASS: Multi-attentional semantic segmentation of LiDAR data for dense top-view understanding. *IEEE Transactions on Intelligent Transportation Systems*, 2022. 2
- [74] Shyam Nandan Rai, Fabio Cermelli, Barbara Caputo, and Carlo Masone. Mask2Anomaly: Mask transformer for universal open-set segmentation. *IEEE Transactions on Pattern Analysis and Machine Intelligence*, 2024. 2
- [75] Minjae Seong, Jisong Kim, Geonho Bang, Hawook Jeong, and Jun Won Choi. MR-Occ: Efficient camera-LiDAR 3D semantic occupancy prediction using hierarchical multi-resolution voxel representation. *arXiv preprint arXiv:2412.20480*, 2024. 2
- [76] Faranak Shamsafar, Samuel Woerz, Rafia Rahim, and Andreas Zell. MobileStereoNet: Towards lightweight deep networks for stereo matching. In *WACV*, 2022. 8
- [77] Hao Shi, Song Wang, Jiaming Zhang, Xiaoting Yin, Guangming Wang, Jianke Zhu, Kailun Yang, and Kaiwei Wang. Offboard occupancy refinement with hybrid propagation for autonomous driving. *IEEE Transactions on Intelligent Transportation Systems*, 2025. 2
- [78] Yiang Shi, Tianheng Cheng, Qian Zhang, Wenyu Liu, and Xinggong Wang. Occupancy as set of points. In *ECCV*, 2024. 2
- [79] Shuran Song, Fisher Yu, Andy Zeng, Angel X Chang, Manolis Savva, and Thomas Funkhouser. Semantic scene completion from a single depth image. In *CVPR*, 2017. 2, 14
- [80] Sanbao Su, Nuo Chen, Chenchen Lin, Felix Juefei-Xu, Chen Feng, and Fei Miao. α -OCC: Uncertainty-aware camera-based 3D semantic scene completion. *arXiv preprint arXiv:2406.11021*, 2024. 2
- [81] Zhiyu Tan, Zichao Dong, Cheng Zhang, Weikun Zhang, Hang Ji, and Hao Li. OVO: Open-vocabulary occupancy. *arXiv preprint arXiv:2305.16133*, 2023. 2
- [82] Pin Tang, Zhongdao Wang, Guoqing Wang, Jilai Zheng, Xiangxuan Ren, Bailan Feng, and Chao Ma. SparseOcc: Rethinking sparse latent representation for vision-based semantic occupancy prediction. In *CVPR*, 2024. 1, 2
- [83] Xiaoyu Tian, Tao Jiang, Longfei Yun, Yucheng Mao, Huitong Yang, Yue Wang, Yilun Wang, and Hang Zhao. Occ3D: A large-scale 3D occupancy prediction benchmark for autonomous driving. In *NeurIPS*, 2023. 15
- [84] Yu Tian, Yuyuan Liu, Guansong Pang, Fengbei Liu, Yuanhong Chen, and Gustavo Carneiro. Pixel-wise energy-biased abstention learning for anomaly segmentation on complex urban driving scenes. In *ECCV*, 2022. 2

- [85] Yonglin Tian, Songlin Bai, Zhiyao Luo, Yutong Wang, Yisheng Lv, and Fei-Yue Wang. MambaOcc: Visual state space model for BEV-based occupancy prediction with local adaptive reordering. *arXiv preprint arXiv:2408.11464*, 2024. 1, 2
- [86] Wenwen Tong, Chonghao Sima, Tai Wang, Li Chen, Silei Wu, Hanming Deng, Yi Gu, Lewei Lu, Ping Luo, Dahua Lin, and Hongyang Li. Scene as occupancy. In *ICCV*, 2023. 2, 15
- [87] Antonin Vobecky, Oriane Siméoni, David Hurych, Spyridon Gidaris, Andrei Bursuc, Patrick Pérez, and Josef Sivic. POP-3D: Open-vocabulary 3D occupancy prediction from images. In *NeurIPS*, 2024. 2
- [88] Tomas Vojir, Tomás Sipka, Rahaf Aljundi, Nikolay Chumerin, Daniel Olmeda Reino, and Jiri Matas. Road anomaly detection by partial image reconstruction with segmentation coupling. In *ICCV*, 2021. 2
- [89] Jiabao Wang, Zhaojiang Liu, Qiang Meng, Liujiang Yan, Ke Wang, Jie Yang, Wei Liu, Qibin Hou, and Ming-Ming Cheng. OPUS: Occupancy prediction using a sparse set. In *NeurIPS*, 2024. 2
- [90] Junming Wang, Wei Yin, Xiaoxiao Long, Xingyu Zhang, Zebin Xing, Xiaoyang Guo, and Qian Zhang. OccRWKV: Rethinking efficient 3D semantic occupancy prediction with linear complexity. *arXiv preprint arXiv:2409.19987*, 2024. 2
- [91] Lubo Wang, Di Lin, Kairui Yang, Ruonan Liu, Qing Guo, Wuyuan Xie, Miaohui Wang, Lingyu Liang, Yi Wang, and Ping Li. Voxel proposal network via multi-frame knowledge distillation for semantic scene completion. In *NeurIPS*, 2024. 2
- [92] Meng Wang, Fan Wu, Ruihui Li, Yunchuan Qin, Zhuo Tang, and Kenli Li. Learning temporal 3D semantic scene completion via optical flow guidance. *arXiv preprint arXiv:2502.14520*, 2025. 2
- [93] Song Wang, Zhongdao Wang, Jiawei Yu, Wentong Li, Bailan Feng, Junbo Chen, and Jianke Zhu. ReliOcc: Towards reliable semantic occupancy prediction via uncertainty learning. *arXiv preprint arXiv:2409.18026*, 2024. 2
- [94] Song Wang, Jiawei Yu, Wentong Li, Hao Shi, Kailun Yang, Junbo Chen, and Jianke Zhu. Label-efficient semantic scene completion with scribble annotations. In *IJCAI*, 2024. 2, 15
- [95] Xiaofeng Wang, Zheng Zhu, Wenbo Xu, Yunpeng Zhang, Yi Wei, Xu Chi, Yun Ye, Dalong Du, Jiwen Lu, and Xingang Wang. OpenOccupancy: A large scale benchmark for surrounding semantic occupancy perception. In *ICCV*, 2023. 15
- [96] Yu Wang and Chao Tong. H2GFormer: Horizontal-to-global voxel transformer for 3D semantic scene completion. In *AAAI*, 2024. 2
- [97] Yi Wei, Linqing Zhao, Wenzhao Zheng, Zheng Zhu, Jie Zhou, and Jiwen Lu. SurroundOcc: Multi-camera 3D occupancy prediction for autonomous driving. In *ICCV*, 2023. 1
- [98] Yuan Wu, Zhiqiang Yan, Zhengxue Wang, Xiang Li, Le Hui, and Jian Yang. Deep height decoupling for precise vision-based 3D occupancy prediction. In *ICRA*, 2025. 2
- [99] Yingda Xia, Yi Zhang, Fengze Liu, Wei Shen, and Alan L. Yuille. Synthesize then compare: Detecting failures and anomalies for semantic segmentation. In *ECCV*, 2020. 2
- [100] Zhaoyang Xia, Youquan Liu, Xin Li, Xinge Zhu, Yuexin Ma, Yikang Li, Yuenan Hou, and Yu Qiao. SCPNet: Semantic scene completion on point cloud. In *CVPR*, 2023. 2
- [101] Yujie Xue, Ruihui Li, Fan Wu, Zhuo Tang, Kenli Li, and Mingxing Duan. Bi-SSC: Geometric-semantic bidirectional fusion for camera-based 3D semantic scene completion. In *CVPR*, 2024. 2
- [102] Yuxiang Yan, Boda Liu, Jianfei Ai, Qinbu Li, Ru Wan, and Jian Pu. PointSSC: A cooperative vehicle-infrastructure point cloud benchmark for semantic scene completion. In *ICRA*, 2024. 15
- [103] Lihe Yang, Bingyi Kang, Zilong Huang, Zhen Zhao, Xiaogang Xu, Jiashi Feng, and Hengshuang Zhao. Depth anything V2. In *NeurIPS*, 2024. 3
- [104] Long Yang, Lianqing Zheng, Wenjin Ai, Minghao Liu, Sen Li, Qunshu Lin, Shengyu Yan, Jie Bai, Zhixiong Ma, and Xichan Zhu. MetaOcc: Surround-view 4D radar and camera fusion framework for 3D occupancy prediction with dual training strategies. *arXiv preprint arXiv:2501.15384*, 2025. 2
- [105] Xuemeng Yang, Hao Zou, Xin Kong, Tianxin Huang, Yong Liu, Wanlong Li, Feng Wen, and Hongbo Zhang. Semantic segmentation-assisted scene completion for LiDAR point clouds. In *IROS*, 2021. 2
- [106] Jiawei Yao, Chuming Li, Keqiang Sun, Yingjie Cai, Hao Li, Wanli Ouyang, and Hongsheng Li. NDC-Scene: Boost monocular 3D semantic scene completion in normalized device coordinates space. In *ICCV*, 2023. 16
- [107] Maosheng Ye, Rui Wan, Shuangjie Xu, Tongyi Cao, and Qifeng Chen. Efficient point cloud segmentation with geometry-aware sparse networks. In *ECCV*, 2022. 5, 6
- [108] Zhangchen Ye, Tao Jiang, Chenfeng Xu, Yiming Li, and Hang Zhao. CVT-Occ: Cost volume temporal fusion for 3D occupancy prediction. In *ECCV*, 2024. 2
- [109] Fengcheng Yu, Haoran Xu, Canming Xia, and Guang Tan. LEAP: Enhancing vision-based occupancy networks with lightweight spatio-temporal correlation. *arXiv preprint arXiv:2502.15438*, 2025. 2
- [110] Zhu Yu, Runmin Zhang, Jiacheng Ying, Junchen Yu, Xiaohai Hu, Lun Luo, Si-Yuan Cao, and Hui-Liang Shen. Context and geometry aware voxel transformer for semantic scene completion. In *NeurIPS*, 2024. 2, 7, 15, 16
- [111] Vitjan Zavrtanik, Matej Kristan, and Danijel Skočaj. Cheating depth: Enhancing 3D surface anomaly detection via depth simulation. In *WACV*, 2024. 2
- [112] Heng Zhai, Jilin Mei, Chen Min, Liang Chen, Fangzhou Zhao, and Yu Hu. WildOcc: A benchmark for off-road 3D semantic occupancy prediction. *arXiv preprint arXiv:2410.15792*, 2024. 15
- [113] Haiming Zhang, Xu Yan, Dongfeng Bai, Jiantao Gao, Pan Wang, Bingbing Liu, Shuguang Cui, and Zhen Li. RadOcc: Learning cross-modality occupancy knowledge through rendering assisted distillation. In *AAAI*, 2024. 2

- [114] Yunpeng Zhang, Zheng Zhu, and Dalong Du. OccFormer: Dual-path transformer for vision-based 3D semantic occupancy prediction. In *ICCV*, 2023. 1, 16
- [115] Yuanfang Zhang, Junxuan Li, Kaiqing Luo, Yiying Yang, Jiayi Han, Nian Liu, Denghui Qin, Peng Han, and Chengpei Xu. V2VSSC: A 3D semantic scene completion benchmark for perception with vehicle to vehicle communication. *arXiv preprint arXiv:2402.04671*, 2024. 15
- [116] Zongkai Zhang, Bin Gao, Jingrui Ye, Huan Jin, Lihui Jiang, and Wenming Yang. CLIP prior-guided 3D open-vocabulary occupancy prediction. *Pattern Recognition*, 2025. 2
- [117] Linqing Zhao, Xiuwei Xu, Ziwei Wang, Yunpeng Zhang, Borui Zhang, Wenzhao Zheng, Dalong Du, Jie Zhou, and Jiwen Lu. LowRankOcc: Tensor decomposition and low-rank recovery for vision-based 3D semantic occupancy prediction. In *CVPR*, 2024. 2
- [118] Xiao Zhao, Bo Chen, Mingyang Sun, Dingkan Yang, Youxing Wang, Xukun Zhang, Mingcheng Li, Dongliang Kou, Xiaoyi Wei, and Lihua Zhang. HybridOcc: NeRF enhanced transformer-based multi-camera 3D occupancy prediction. *IEEE Robotics and Automation Letters*, 2024. 2
- [119] Jilai Zheng, Pin Tang, Zhongdao Wang, Guoqing Wang, Xiangxuan Ren, Bailan Feng, and Chao Ma. VEON: Vocabulary-enhanced occupancy prediction. In *ECCV*, 2024. 2
- [120] Lianqing Zheng, Jianan Liu, Runwei Guan, Long Yang, Shouyi Lu, Yuanzhe Li, Xiaokai Bai, Jie Bai, Zhixiong Ma, Hui-Liang Shen, and Xichan Zhu. Doracamom: Joint 3D detection and occupancy prediction with multi-view 4D radars and cameras for omnidirectional perception. *arXiv preprint arXiv:2501.15394*, 2025. 2
- [121] Yupeng Zheng, Xiang Li, Pengfei Li, Yuhang Zheng, Bu Jin, Chengliang Zhong, Xiaoxiao Long, Hao Zhao, and Qichao Zhang. MonoOcc: Digging into monocular semantic occupancy prediction. In *ICRA*, 2024. 1, 2
- [122] Zheyuan Zhou, Le Wang, Naiyu Fang, Zili Wang, Lemiao Qiu, and Shuyou Zhang. R3D-AD: Reconstruction via diffusion for 3D anomaly detection. In *ECCV*, 2024. 2
- [123] Benjin Zhu, Zhe Wang, and Hongsheng Li. nuCraft: Crafting high resolution 3D semantic occupancy for unified 3D scene understanding. In *ECCV*, 2024. 2, 15
- [124] Hao Zou, Xuemeng Yang, Tianxin Huang, Chujuan Zhang, Yong Liu, Wanlong Li, Feng Wen, and Hongbo Zhang. Up-to-down network: Fusing multi-scale context for 3D semantic scene completion. In *IROS*, 2021. 2

7. Out-of-Distribution Semantic Occupancy Prediction Datasets and Metrics

Datasets. We evaluate our OccOoD on four datasets: SemanticKITTI [3], SSCBench-KITTI-360 [52], VAA-KITTI, and VAA-KITTI-360. The evaluation is performed within a spatial volume defined as 51.2 meters forward, 25.6 meters laterally (left and right), and 6.4 meters vertically above the vehicle. This volume is discretized into a 3D voxel grid with dimensions $256 \times 256 \times 32$, where each voxel has a uniform size of 0.2 meters along each axis. SemanticKITTI provides RGB images with a resolution of 1226×370 pixels, encompassing 20 distinct semantic classes (19 classes plus one free space class). The dataset is partitioned into 10 training sequences, 1 validation sequence, and 11 testing sequences. Similarly, SSCBench-KITTI-360 comprises 7 training sequences, 1 validation sequence, and 1 testing sequence, featuring 19 semantic classes (18 classes plus one free space class) with input RGB images at a resolution of 1408×376 pixels.

As summarized in Table 6, the VAA-KITTI and VAA-KITTI-360 datasets, derived from SemanticKITTI [3] and SSCBench-KITTI-360 [52] respectively, each include 500 test images that preserve the original resolution while introducing an additional anomaly class. Specifically, VAA-KITTI is generated by selecting sequences 07, 09, and 10 from the 10 training sequences of the SemanticKITTI [3] as the foundation, using the proposed *Synthetic Anomaly Integration Pipeline*. Similarly, VAA-KITTI-360 is constructed based on the testing sequence of the SSCBench-KITTI-360 [52], also leveraging the *Synthetic Anomaly Integration Pipeline* for anomaly synthesis.

While both VAA-KITTI and VAA-KITTI-360 share the same set of anomaly object categories, their distributions differ significantly. In VAA-KITTI-360, the proportions of anomaly types are relatively balanced, whereas in VAA-KITTI, the distribution is more extreme. This design choice aims to validate the robustness of our method under varying anomaly distribution scenarios, ensuring its adaptability to both uniform and skewed anomaly occurrences.

Metrics. Following [79], we evaluate performance using the Intersection over Union (IoU) metric for scene completion and the mean IoU (mIoU) metric for semantic scene completion. For out-of-distribution (OoD) detection, in addition to the previously mentioned AuPRC_r , we also employ the Area Under the Receiver Operating Characteristic curve (AuROC) metric, which is calculated by evaluating the True Positive Rate (TPR) against the False Positive Rate (FPR) at various threshold levels. We provide a detailed explanation below. The TPR, FPR, precision, and recall can be defined as:

$$\text{TPR} = \frac{\text{TP}}{\text{TP} + \text{FN}}, \quad (16)$$

$$\text{FPR} = \frac{\text{FP}}{\text{FP} + \text{TN}}, \quad (17)$$

where TP, FP, and FN denote true positives, false positives, and false negatives. The AuROC is computed as:

$$\text{AuROC} = \int_0^1 \text{TPR}(\text{FPR}) d\text{FPR}. \quad (18)$$

For the AuPRC_r metric, we mitigate the impact of absolute positional errors in predictions by dilating the ground-truth labels to create anomaly regions. This process involves expanding the original labels outward by 4, 5, and 6 voxels, corresponding to regions of $0.8m$, $1.0m$, and $1.2m$, respectively. To ensure that the modification fulfills its intended purpose while maintaining fairness and accuracy in evaluation, we carefully account for the resulting increases in false negatives and true negatives.

8. Implementation Details

Details of the BEV Encoder. As shown in Fig. 6, each BEV encoder consists of convolution blocks, each followed by a VRWKV block [26], along with an ARF module [65]. **Training Setup.** We train OccOoD for 40 epochs on 4 RTX3090 GPUs with a batch size of 4, using AdamW [60] with an initial learning rate of $2e-4$ and weight decay of $1e-2$. The model, with 38 million parameters, has two configurations: OccOoD-S, which uses the current image, and OccOoD-T, which integrates the current and previous 4 images, following SGN [66].

9. Additional Quantitative Results

Due to space limitations in the main text, we provide additional semantic occupancy prediction results of OccOoD on the SSCBench-KITTI-360 benchmark and the VAA-KITTI-360 dataset in Table 7 and Table 8, respectively. Across these evaluations, OccOoD consistently surpasses baseline methods, particularly excelling in the accurate identification of complex regions such as road boundaries, dynamic objects, and anomalous areas. This improvement is largely attributed to our Voxel-BEV Progressive Fusion (VBPF) design, which effectively leverages the spatial characteristics of BEV representations while preserving fine-grained details from voxel-based features.

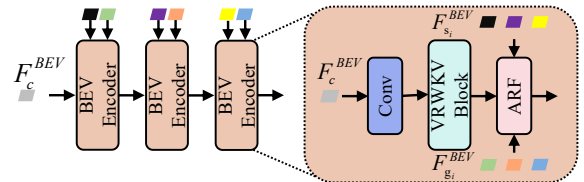


Figure 6. Details of the BEV encoder in the UNet-like architecture.

Datasets	Year	OoD Object	Domain	Real-World	Modality	#Classes	Voxel Size
Road Anomaly [55]	2019						
Fishscapes L&F [8]	2019						
Fishscapes Static [8]	2019	✓	2D			2	-
StreetHazards [33]	2019						
SMIYC RA-21 [17]	2021						
SMIYC RO-21 [17]	2021						
SemanticKITTI [3]	2019					28	256×256×32
SemanticPOSS [72]	2020					14	-
Occ3D-nuScenes [83]	2023					16	200×200×16
Occ3D-Waymo [83]	2023					14	200×200×32
nuScenes-Occupancy [95]	2023	✗	3D			16	512×512×40
OpenOcc [86]	2023					16	200×200×16
SSCBench-KITTI360 [52]	2024					19	256×256×32
nuCraft [123]	2024					16	1024×1024×80
PointSSC [102]	2024					9	-
WildOcc [112]	2024					20	256×256×32
V2VSSC [115]	2024					6	128×128×20
ScribbleSC [94]	2024					19	256×256×32
VAA-KITTI	2025	✓	3D			29	256×256×32
VAA-KITTI-360	2025					20	256×256×32

Table 6. Comparison of datasets for anomaly segmentation and semantic scene completion. Abbreviations: ✓ (There are OoD objects in the scene), ✗ (No OoD objects in the scene), (Real-World Data), (Synthetic Data), (Camera), (LiDAR).

Method	IoU	car	bicycle	motorcycle	truck	other-veh.	person	road	parking	sidewalk	other-gmd.	building	fence	vegetation	terrain	pole	traf.sign	other-struct.	other-obj.	mIoU
		■	■	■	■	■	■	■	■	■	■	■	■	■	■	■	■	■	■	
SSCBench-KITTI-360																				
VoxFormer [51]	38.76	17.84	1.16	0.89	4.56	2.06	1.63	47.01	9.67	27.21	2.89	31.18	4.97	28.99	14.69	6.51	6.92	3.79	2.43	11.91
SGN [66]	<u>47.06</u>	29.03	3.43	2.90	10.89	5.20	2.99	58.14	15.04	36.40	4.43	42.02	7.72	38.17	<u>23.22</u>	<u>16.73</u>	16.38	9.93	5.86	18.25
Symphonies [41]	44.12	30.02	1.85	5.90	25.07	12.06	8.20	54.94	13.83	32.76	6.93	35.11	8.58	<u>38.33</u>	11.52	14.01	9.57	14.44	11.28	<u>18.58</u>
CGFormer [110]	48.07	<u>29.85</u>	<u>3.42</u>	<u>3.96</u>	<u>17.59</u>	<u>6.79</u>	<u>6.63</u>	63.85	17.15	40.72	<u>5.53</u>	<u>42.73</u>	<u>8.22</u>	38.80	24.94	16.24	<u>17.45</u>	<u>10.18</u>	6.77	20.05
OccOoD (Ours)	46.93	28.51	2.95	0.94	9.48	4.57	2.99	<u>58.91</u>	<u>16.17</u>	<u>37.04</u>	5.34	42.99	7.83	37.41	23.01	17.47	18.87	8.94	<u>7.16</u>	18.37
VAA-KITTI-360																				
SGN-S [66]	39.68	20.68	0.05	0.00	0.00	2.92	0.00	47.59	14.66	24.71	2.56	32.83	3.52	28.68	11.63	7.44	8.67	4.29	5.52	11.99
OccOoD-S (Ours)	39.26	22.84	0.00	0.00	0.00	3.54	0.58	49.09	14.65	27.84	3.41	32.59	1.55	27.46	11.46	8.42	12.30	3.63	6.49	12.55

Table 7. Quantitative results on the SSCBench-KITTI360 test set [52] and VAA-KITTI-360. The results for counterparts are provided in [52]. The best and the second best results are in **bold** and underlined, respectively.

10. Other OoD Detection Methods

Energy-Based Anomaly Score: The energy-based anomaly score is computed as:

$$S_{\text{energy}}(v_i) = -\log \sum_{k \in \mathcal{K}} \exp(l(k|v_i)), \quad (19)$$

where \mathcal{K} represents the set of possible classes, and $l(k|v_i)$ denotes the unnormalized log-probability (logit) that voxel

v_i is predicted to be of class k . The formulation employs the log-sum-exp operation to compute a scalar energy value, reflecting the model’s overall prediction confidence. Higher energy values correspond to lower confidence, signaling potential anomalous regions.

Posterior Probability-Based Anomaly Score: The posterior probability-based anomaly score is computed as:

$$S_{\text{postpro}}(v_i) = 1 - \max_{k \in \mathcal{K}} l(k|v_i). \quad (20)$$

Method	IoU	road	sidewalk	parking	otherground	building	car	truck	bicycle	motorcycle	othervehicle	vegetation	trunk	terrain	person	bicyclist	motorcyclist	fence	pole	trafficsign	mIoU
		■	■	■	■	■	■	■	■	■	■	■	■	■	■	■	■	■	■	■	
MonoScene [12]	37.12	57.47	27.05	15.72	0.87	14.24	23.55	7.83	0.20	0.77	3.59	18.12	2.57	30.76	1.79	1.03	0.00	6.39	4.11	2.48	11.50
TPVFormer [37]	35.61	56.50	25.87	20.60	0.85	13.88	23.81	8.08	0.36	0.05	4.35	16.92	2.26	30.38	0.51	0.89	0.00	5.94	3.14	1.52	11.36
VoxFormer [51]	44.02	54.76	26.35	15.50	0.70	17.65	25.79	5.63	0.59	0.51	3.77	24.39	5.08	29.96	1.78	<u>3.32</u>	0.00	7.64	7.11	4.18	12.35
OccFormer [114]	36.50	58.85	26.88	19.61	0.31	14.40	25.09	25.53	0.81	1.19	8.52	19.63	3.93	32.62	2.78	2.82	0.00	5.61	4.26	2.86	13.46
NDC-scene [106]	37.24	59.20	28.24	<u>21.42</u>	1.67	14.94	26.26	14.75	1.67	2.37	7.73	19.09	3.51	31.04	<u>3.60</u>	2.74	0.00	6.65	4.53	2.73	12.70
SGN [66]	<u>46.21</u>	59.10	29.41	19.05	0.33	<u>25.17</u>	33.31	6.03	0.61	0.46	9.84	28.93	9.58	<u>38.12</u>	0.47	0.10	0.00	9.96	13.25	<u>7.21</u>	15.32
Symphonies [41]	41.92	57.11	27.79	16.97	<u>1.22</u>	21.74	29.08	14.36	<u>3.75</u>	3.06	14.38	25.32	6.87	29.70	4.27	2.76	0.08	8.71	9.5	6.24	14.89
CGFormer [110]	45.99	65.51	32.31	20.82	0.16	23.52	34.32	19.44	4.61	<u>2.71</u>	7.67	26.93	8.83	39.54	2.38	4.08	0.00	9.20	10.67	7.84	16.89
OccOoD (Ours)	46.83	<u>60.87</u>	<u>32.16</u>	23.52	0.06	26.54	<u>33.51</u>	<u>25.17</u>	0.65	1.00	<u>11.84</u>	<u>28.43</u>	<u>8.90</u>	36.96	0.44	0.16	0.00	<u>9.94</u>	<u>13.00</u>	6.03	<u>16.80</u>

Table 8. Quantitative results on the SemanticKITTI validation set [3]. The best and the second best results are in **bold** and underlined, respectively.

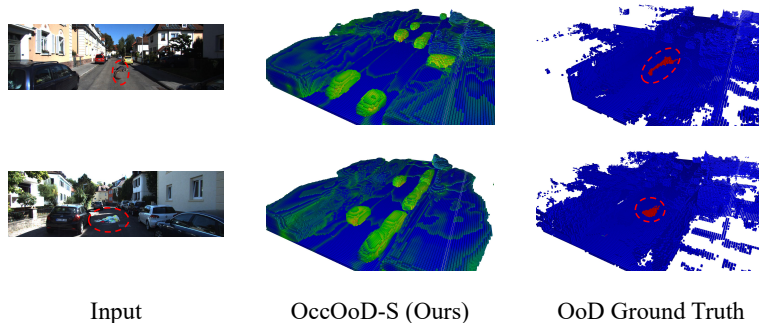


Figure 7. Failure cases.

This score measures the deviation from the most confident prediction by subtracting the maximum logit value from 1. A higher score indicates that the model’s prediction is less certain, suggesting potential anomalies.

The two anomaly scores offer complementary views of the model’s confidence. The energy-based score (Eq. (19)) aggregates across all classes, reflecting global prediction uncertainty, while the posterior probability-based score (Eq. (20)) focuses on the most likely class, providing a localized confidence measure. However, both scores are insensitive to semantic categories, as they fail to fully capture the semantic-specific uncertainty and the distinct characteristics of different classes in voxel space.

11. Failure Case Analysis

We present two failure cases of out-of-distribution semantic occupancy prediction in Fig. 7, where the misclassification of anomalous objects as empty space or road is primarily attributed to their relatively low height. A potential solution to this issue is to enhance the model’s ability to accurately predict the occupancy of small or low-height objects, ensuring better recognition and representation of such anomalies

in the scene.